JACS
JOURNAL OF THE AMERICAN CHEMICAL SOCIETY
Article
pubs.acs.org/JACS

III–V Nanocrystals Capped with Molecular Metal Chalcogenide Ligands: High Electron Mobility and Ambipolar Photoresponse

Wenyong Liu,[†,§] Jong-Soo Lee,[†,§] and Dmitri V. Talapin*[,†,‡]

[†]Department of Chemistry and James Frank Institute, University of Chicago, Illinois 60637, United States
[‡]Center for Nanoscale Materials, Argonne National Lab, Argonne, Illinois 60439, United States

Supporting Information

ABSTRACT: In this work, we synthesized InP and InAs nanocrystals (NCs) capped with different inorganic ligands, including various molecular metal chalcogenide complexes (MCCs) and chalcogenide ions. We found that MCCs and chalcogenide ions can quantitatively displace organic ligands from the surface of III–V NCs and serve as the inorganic capping groups for III–V NC surfaces. These inorganic ligands stabilize colloidal solutions of InP and InAs NCs in polar solvents and greatly facilitate charge transport between individual NCs. Charge transport studies revealed high electron mobility in the films of MCC-capped InP and InAs NCs. For example, we found that bridging InAs NCs with $Cu_7S_4^-$ MCC ligands can lead to very high electron mobility exceeding 15 $cm^2/(V\ s)$. In addition, we observed unprecedented ambipolar (positive/negative) photoresponse of MCC-capped InAs NC solids that changed sign depending on the ligand chemistry, illumination wavelength, and doping of the NC solid. For example, the sign of photoconductance of InAs NCs capped with $Cu_7S_4^-$ or $Sn_2S_6^{4-}$ ions converted from positive at 0.80 and 0.95 eV to negative at 1.27 and 1.91 eV. We propose an explanation of this unusually complex photoconductivity of InAs NC solids.

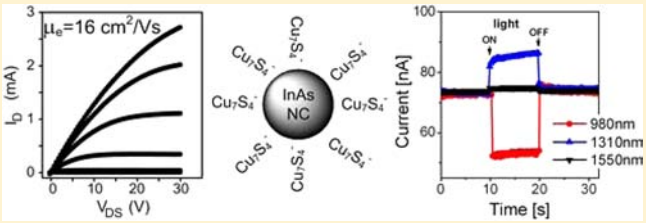

1. INTRODUCTION

III–V semiconductors such as GaAs, InP, and InAs combine direct band gap with very high mobility, reliable p- and n-type doping, and other characteristics that make them excellent materials for various electronic and photonic applications.[1−3] The fastest commercial transistors and the most efficient solar cells employ III–V semiconductors. At the same time, despite all the benefits, technological difficulties associated with growing and processing single crystals do not allow III–V materials to successfully compete with Si and II–VI semiconductors for large consumer markets. As a possible solution, colloidal nanocrystals (NCs) such as InAs and InP can be used as a cost-efficient alternative to III–V single crystals for applications in photovoltaics, photo detectors, field-effect transistors (FETs),[4,5] and light-emitting diodes (LEDs).[6,7] Moreover, many III–V nanomaterials also show relatively low toxicity (e.g., InP) that provides an important advantage over Cd- and Pb-based NCs. From this perspective, switching to InP and InAs NCs instead of CdSe and PbSe NCs would constitute a significant step forward in the manufacturability of functional nanomaterials and their transitioning from laboratory to real-world applications.

Most device applications of semiconductor NCs require efficient injection or extraction of charge carriers. Traditional colloidal synthesis of III–V NCs requires the use of surface ligands with long hydrocarbon tails (e.g., tri-*n*-octylphosphine (TOP) or myristate) that form insulating shells around each NC and negatively affect the charge transport.[8] Removal of organic surfactants via thermal or chemical treatments often leads to surface traps and uncontrollable sintering.[9] A more promising approach is to chemically treat NCs with small or conductive ligands.[10] These techniques have been originally developed for II–VI (e.g., CdSe)[11−14] and IV–VI (e.g., PbSe)[15−17] NCs. There are only a couple of reported charge transport studies for InAs NCs that used either postdeposition ligand exchange treatment of InAs NCs with ethanedithiol[18] or solution ligand exchange of TOP capped InAs NCs with aniline followed by postdeposition cross-linking with ethylenediamine (EDA).[5] Such treatments converted highly insulating organic-capped InAs NCs into semiconducting NC solids with the charge carrier mobility on the order of 10^{-5} $cm^2/(V\ s)$.[12] Such mobilities show certain promise but are not yet sufficient for practical applications. Equally important, small organic ligands often are chemically unstable or volatile and therefore impart instability to the electronic properties of NC solids.

It has been recently shown that insulating organic ligands can be replaced with the inorganic ligands, such as molecular metal chalcogenide complexes (MCCs; e.g., $Sn_2S_6^{4-}$, $In_2Se_4^{2-}$, etc.),[19,20] chalcogenide ions (S^{2-}, Se^{2-}, and Te^{2-}),[17] and other charged small anions such as SCN^-.[21] These developments in the surface chemistry of II–VI and IV–VI NCs enabled strong electronic coupling between individual NCs and opened new prospects for electronic and optoelectronic applications of NC solids.[22,23] In this contribution, we explore the application of inorganic ligands to more covalent III–V

Received: August 17, 2012
Published: December 26, 2012

 © 2012 American Chemical Society dx.doi.org/10.1021/ja308200f | J. Am. Chem. Soc. 2013, 135, 1349−1357

NCs. To the best of our knowledge, this is the first systematic study of all-inorganic III–V colloidal NCs. We show that this advance in the surface chemistry provides about a 10^6-fold improvement of the electron mobility in InAs NC films compared to the mobility achieved with organic ligands. Such mobility improvements significantly expand potential application areas for III–V nanomaterials. Our work also demonstrates and investigated the unprecedented ambipolar photoresponse of InAs NCs. To the best of our knowledge, this is the first observation of such behavior for semiconductor NCs.

2. EXPERIMENTAL SECTION

2.1. Synthesis of Colloidal NCs. A modified recipe of Guzelian et al. was used to synthesize InAs NCs capped with TOP.[17] InP NCs capped with myristic acid were synthesized following a slightly modified recipe reported in refs 24 and 25. Detailed synthetic protocols are provided in the Supporting Information.

2.2. Synthesis of Molecular MCCs. $(N_2H_4)_2(N_2H_5)_2In_2Se_4$, $(N_2H_5)_4Sn_2S_6$, $(N_2H_4)(N_2H_5)_4Sn_2Se_6$, $(N_4H_9)Cu_7S_4$, and $(N_2H_4)_x(N_2H_5)_3(In_2Cu_2Se_4S_3)$ were synthesized as described in refs 26–29. Additional details are provided in the Supporting Information.

2.3. Exchange of Organic Ligands on As-synthesized III–V NCs with MCCs. All ligand exchange procedures were carried out in a nitrogen-filled glovebox (1–2 ppm O_2 and H_2O levels) using anhydrous solvents. The molar ratio of MCC to NC materials during the ligand exchange was around 1:1. In a typical example for 5 nm InAs NCs, 2 mL of InAs NC solution in hexane (4.2 mg/mL) was loaded on top of a 2 mL solution of $(N_4H_9)Cu_7S_4$ (15.9 mg/mL) in N_2H_4 (Figure 1a). The solution was stirred for about 30 min to 1 h until the upper organic phase turned colorless and the lower hydrazine phase turned dark. The organic phase was carefully removed, and the hydrazine phase was purified by washing three times with anhydrous toluene. MCC-capped InAs NCs were precipitated from hydrazine solution by adding a minimal amount of anhydrous acetonitrile (approximately 50% of NC solution volume), collected by centrifugation, redissolved into hydrazine, and filtered through a 0.2 μm PTFE filter.

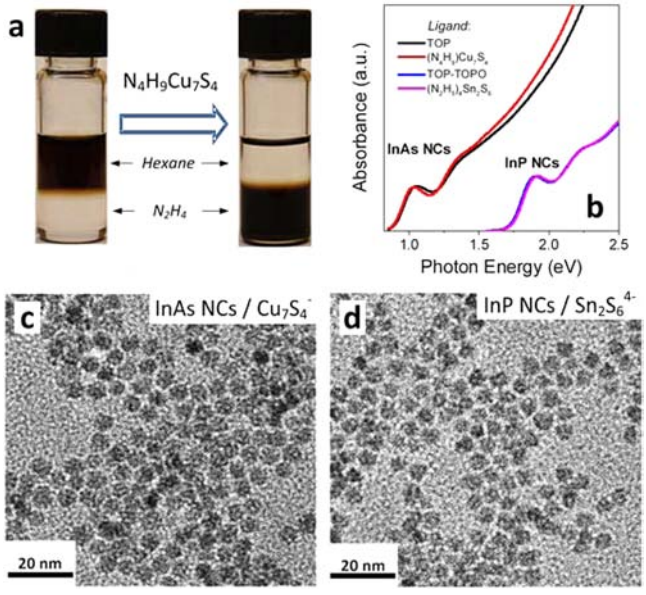

Figure 1. (a) Black solution of InAs NCs undergoes the phase transfer from hexane to hydrazine in the presence of MCC ligands. (b) Absorption spectra of InAs NCs capped with TOP in toluene and $(N_2H_5)Cu_7S_4$ in hydrazine and InP NCs capped with TOP and TOPO in toluene and $(N_2H_5)_4Sn_2S_6$ in hydrazine. (c) TEM image of InAs NCs capped with $(N_2H_5)Cu_7S_4$. (d) TEM image of InP capped with $(N_2H_5)_4Sn_2S_6$.

Exchange of organic ligands on as-synthesized III–V NCs with S^{2-} and other metal-free inorganic ligands was carried out following the protocols reported in ref 17.

2.4. FET Device Fabrication. Samples for electrical measurements were prepared by depositing thin 10–30 nm (±20%) films by spin-coating MCC-capped NCs onto highly doped Si wafers with a 100 nm thick layer of SiO_2 thermal gate oxide. The oxide surface was hydrophilized by oxygen plasma or piranha treatment prior to NC deposition. The thickness of the NC film was controlled by adjusting the concentration of the NC solution and substrate spinning rate. Typically, a 25–30 nm thick NC film can be fabricated by spin-coating a ~30 mg/mL InAs NC solution in hydrazine at the spinning rate of 600 rpm for 6 s followed by 2000 rpm for 30 s (KW-4A spin-coater, Chemat Tech, Inc.). All device fabrication steps were carried out under dry nitrogen atmosphere. As-deposited NC films were dried at 80 °C for 30 min followed by annealing at 200 °C for 1 h using a hot-plate or at 350 °C for 5 s using a rapid thermal annealing (RTA) system to remove the solvent and transform MCC ligands into metal chalcogenide inter-NC linkers.[22,30] Source and drain Al (~1000 Å thick) electrodes were directly patterned on top of annealed NC films using a shadow mask.

2.5. Electrical Measurements. The electrical measurements were performed using an Agilent B1500A semiconductor parameter analyzer under dry nitrogen atmosphere. All FET measurements were carried out under quasi-static conditions with typical voltage scan rates of 0.12 V s^{-1} and 40 mV s^{-1} for I_D–V_G and I_D–V_{DS} scans, respectively. The electron mobility was calculated from the slope of the drain current (I_D) versus V_G measured when the gate voltage was scanned in the forward direction (i.e., from negative to positive). For an n-type FET, this measurement typically provides a conservative estimate for the field effect mobility.

2.6. Photoconductivity Measurements. For the photoconductivity measurements, close-packed films of InAs NCs capped with different MCC ligands ($In_2Se_4^{2-}$, $Cu_7S_4^-$, $Sn_2S_6^{4-}$, $Sn_2Se_6^{4-}$, and $In_2Cu_2Se_4S_3^{3-}$) or InP NCs capped with $In_2Se_4^{2-}$, $Sn_2S_6^{4-}$, or $Sn_2Se_6^{4-}$ ligands were deposited on Si wafers with a thick layer of 100 nm SiO_2 gate oxide with Ti/Au (5/45 nm) electrodes patterned by photolithography. The surfaces of the substrates were hydrophilized by oxygen plasma treatment. As-deposited NC films were dried at 80 °C for 30 min following by the annealing at 200 °C for 1 h for MCC-capped InAs NCs and at 250 °C for 30 min for MCC-capped InP NCs. For the photoresponse versus time (i–t) measurements, the devices were biased using a Keithley 2400 source meter controlled by a LabView program. The photocurrent was measured under illumination with four different CW LEDs emitting at 650 nm (1.91 eV), 980 nm (1.27 eV), 1310 nm (0.95 eV), and 1550 nm (0.80 eV), respectively.

3. RESULTS AND DISCUSSION

3.1. Synthesis of Inorganically Capped InAs and InP NCs. For synthesis of hydrazinium chalcogenidometallates (MCCs used in this work), we used the Mitzi's approach based on direct dissolution metals or metal chalcogenides in neat N_2H_4 in the presence of elemental chalcogens.[17–21] The ligand exchange was carried out through the phase transfer procedure in which TOP-capped InAs NCs or myristate-capped InP NCs dispersed in nonpolar solvent (hexane or toluene) were transferred into the N_2H_4 phase after all organic ligands at the NC surface were replaced with MCCs (Figure 1a). To explore the versatility of such ligand exchange, five different hydrazinium chalcogenidometallates were studied: $(N_2H_4)_2(N_2H_5)_2In_2Se_4$, $(N_2H_5)_4Sn_2S_6$, $(N_2H_4)(N_2H_5)_4Sn_2Se_6$, $(N_2H_4)(N_2H_5)Cu_7S_4$, and $(N_2H_4)_x(N_2H_5)_3\{In_2Cu_2Se_4S_3\}$. TOP-capped InAs NCs worked well with all the above MCCs whereas InP NCs could be stabilized with all MCC ligands except $(N_4H_9)Cu_7S_4$ that apparently etched InP NCs.

dx.doi.org/10.1021/ja308200f | J. Am. Chem. Soc. 2013, 135, 1349–1357

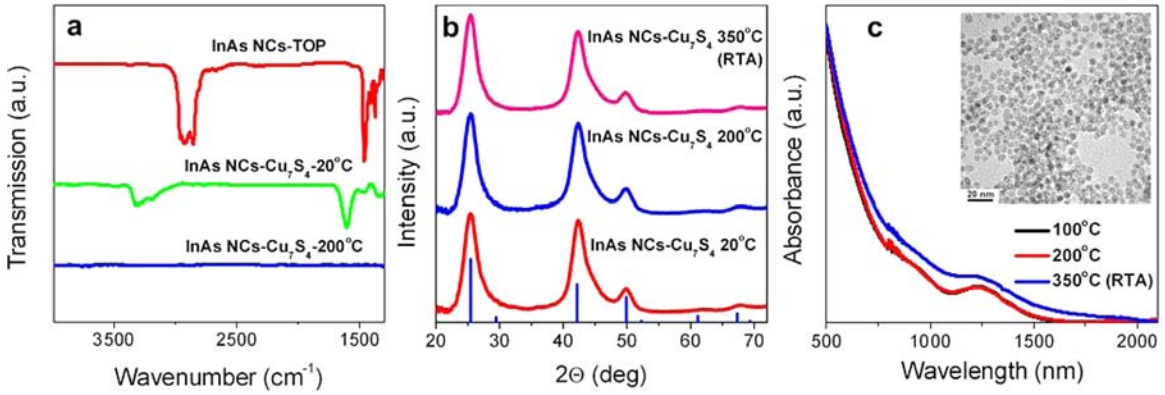

Figure 2. (a) FTIR spectra of InAs NCs capped with TOP (red line) and $(N_2H_5)Cu_7S_4$ ligands before (green line) and after heating to 200 °C (blue line). The disappearance of C−H absorption lines between 3000 and 2800 cm^{-1} indicates the removal of the organic ligands. The vanishing of N−H stretching absorption bands between 3400 and 3000 cm^{-1} indicates thermal decomposition of the inorganic ligands at 200 °C. (b) The X-ray diffraction patterns of InAs NCs capped with $(N_2H_5)Cu_7S_4$ at room temperature (black line), after annealing at 200 °C (blue line), and after RTA at 350 °C for 5 s (red line). (c) Absorption spectra collected using an integrating sphere for thin films of 4.5 nm InAs NCs capped with $(N_2H_5)Cu_7S_4$ ligands annealed at 100 °C (black line), 200 °C (red line) using a hot-plate, and 350 °C for 5 s using a RTA system (blue line). The inset shows a TEM image of 4.5 nm InAs NCs capped with $(N_2H_5)Cu_7S_4$ after RTA annealing at 350 °C for 5 s.

High purity of original organic-capped NCs was important to the success of the ligand exchange process and to the performance of the NC-based FET devices. The InAs and InP NCs dissolved in toluene solution were washed by carefully adding a minimum amount of ethanol needed to precipitate the NC colloid. The NCs were collected by centrifugation, and the supernatant was decanted. Precipitated NCs were redispersed into toluene solution. Three cycles of washing were employed to carefully remove all unreacted precursors, byproducts, and free ligands from the NC solution. The type of original organic ligand on the NCs also influenced the results of the ligand exchange. For example, InP NCs originally capped with TOP/TOPO precipitated out in N_2H_4 after ligand exchange with MCCs. Among these precipitates, only InP NCs capped with $(N_2H_5)_4Sn_2S_6$ could redissolve into formamide (FA), which has much higher dielectric constant (ε = 106) compared to N_2H_4 (ε = 55). On the other hand, the ligand exchange can be performed with all the MCCs except $(N_4H_9)Cu_7S_4$ in *N*-methyl formamide (NMF) instead of N_2H_4 due to the extremely high NMF dielectric constant (ε = 182). The attempts to treat TOP/TOPO-capped InP NCs with $NOBF_4$ to get ligand-free NCs following the approach of Murray et al.[31] and then to perform ligand exchange with MCCs was not successful because $NOBF_4$ etched the InP NCs. Simple chalcogenide ligands (S^{2-}, Se^{2-}, and Te^{2-}) worked well with InAs and InP NCs regardless of the original organic surfactants.[32]

The time required to complete the ligand exchange ranged from a few minutes to several hours. As confirmed by transmission electron microscopy (TEM) images, the original size and shape of the InAs (~4.8 ± 0.5 nm) and InP NCs (3.8 ± 0.4 nm) were preserved after the ligand exchange with sizes of InAs of ~4.6 ± 0.5 nm and of InP of ~3.8 ± 0.4 nm, respectively, as shown in Figures 1c,d and S1 (Supporting Information). III−V NCs also retained their electronic structure and size distribution as seen from the excitonic features in the absorption spectra of $Cu_7S_4^-$-capped InAs and of $Sn_2S_6^{4-}$-capped InP NCs (Figure 1b). Fourier transform IR (FTIR) spectra taken before and after ligand exchange for $Cu_7S_4^-$-capped InAs and $Sn_2S_6^{4-}$-capped InP NCs showed that the strong absorption bands at 2800−3000 cm^{-1} arising from characteristic C−H stretching of original hydrocarbon ligands were completely diminished after the ligand exchange reaction (Figures 2a and S2 (Supporting Information) for InAs and InP NCs, respectively), confirming complete removal of organic surfactants from the NC surface. The weak broad absorption bands characteristic of the N−H stretching appear at 3200−3300 cm^{-1}. These could originate both from N_2H_4 molecules coordinatively bound to the NC surface or MCC ligands and from $N_2H_5^+$ counterions in close proximity to negatively charged MCC ligands. The attachment of negatively charged MCC ligands to the surface of InAs NCs resulted in a negative −61.3 mV ξ-potential (Figure S3, Supporting Information) sufficient to provide electrostatic stabilization of colloidal NC solutions in N_2H_4 and other polar solvents. Dynamic light scattering (DLS) measurements shown in Figure S4 (Supporting Information) confirm the colloidal stability of MCC-capped III−V NCs.

As-synthesized InP NCs show very weak photoluminescence (PL) due to the presence of midgap trap states at the NC surface.[33] The exchange of inorganic ligands with MCCs or S^{2-} ions did not result in significant improvement of PL efficiency. However, PL efficiency of InP NCs can be improved by several orders of magnitude by photochemical etching of the NC surface with HF that selectively removes charge-trapping states from the surface of InP NCs.[33] We applied this treatment to InP NCs capped with S^{2-} or $Sn_2S_6^{4-}$ ligands. These obtained colloidal solutions of InP NCs showed a strong band edge PL with a quantum efficiency of ~5%.

For charge transport and photoconductivity measurements, we prepared close-packed films of InP and InAs NCs capped with different inorganic ligands. These measurements were performed after annealing the NC films, for example, at 200 °C. We therefore applied various techniques to probe morphological and electronic properties of III−V NC arrays before and after the heat treatment. Thermogravimetric analysis measurements on $Cu_7S_4^-$-capped InAs NCs showed 2.13% and 3.3% weight loss at 200 and 350 °C, respectively, which is much smaller than the weight losses (12.4%) observed for pure $(N_4H_9)Cu_7S_4$ ligands (Figure S5a, Supporting Information). The weight loss at 200 °C was caused by the elimination of weakly bound and thermally unstable N_2H_4 and $N_2H_5^+$, in agreement with FTIR data showing that the N−H stretching

dx.doi.org/10.1021/ja308200f | *J. Am. Chem. Soc.* 2013, 135, 1349−1357

bands at 3200−3300 cm^{-1} disappear after annealing at 200 °C for 30 min (Figures 2a and S2 (Supporting Information) for InAs and InP NCs, respectively).

The $(N_4H_9)Cu_7S_4$ MCC has a relatively low decomposition temperature (~120 °C, Figure S5b, Supporting Information) compared to other hydrazinium chalcogenidometallates due to relatively weak hydrogen bonding between $Cu_7S_4^-$ anions and hydrazinium and hydrazine species.[14] Decomposition of a pure MCC results in the formation of Cu_2S. It is logical to assume that a very thin layer of Cu_2S forms between InAs NCs after annealing at 200 °C. This transformation did not result in any detectable changes of the absorption spectrum of the NC film as shown in Figure 2c. The X-ray diffraction (XRD) patterns of $Cu_7S_4^-$-capped InAs NCs and $Sn_2S_6^{4-}$-capped InP NCs were identical before and after annealing at 200 °C and showed no peaks from Cu_2S or SnS_2 phases as well as other phases except InAs or InP (Figures 2b and S6 (Supporting Information) for InAs and InP NCs, respectively) suggesting the absence of phase separation between NCs and MMC ligands. Such behavior is similar to that observed for MCC- and S^{2-}-capped II−VI NCs.[19,22] At the same time, we noticed that inorganically capped III−V NCs are much more stable against sintering compared to CdSe or lead chalcogenide NCs. For example, even short-time annealing at 350 °C using a RTA system resulted in the disappearance of the excitonic features in the absorption of $In_2Se_4^{2-}$-capped CdSe NC solids.[30] In contrast, both InAs and InP NCs showed only minor changes in the absorption spectra after annealing at 350 °C for 5 s. Thus, the absorption spectra of InAs NCs showed no changes after annealing at 200 °C for 30 min while some broadening of the excitonic peak was observed after heating to 350 °C for 5 s (Figure 2c). The XRD patterns of InAs NC solids annealed at 350 °C for 5 s showed no obvious narrowing of the diffraction peaks (Figure 2b) that could be interpreted as the absence of NC sintering. The TEM images of inorganically capped InAs NCs annealed at 350 °C for 5 s showed separated nonsintered NCs (inset in Figure 2c). The films of ~4 nm InP NCs capped with $Sn_2S_6^{4-}$ ligands annealed at 350 °C for 5−15 s also revealed no changes in the absorption spectra and XRD patterns (Figure S7, Supporting Information). The stability of MCC-capped III−V NCs against sintering could be explained by stabilization of grain boundaries between III−V crystallites by metal chalcogenide layers. Further studies will be needed to elucidate the microscopic mechanism of grain boundary stabilization in MCC-capped III−V nanostructures.

3.2. Charge Transport in the Arrays of MCC-capped InAs and InP NCs. The electronic properties of NC-based functional materials are determined by the ability of charge carriers to move across inter-NC boundaries. Strong inter-NC coupling is crucial for the performance of electronic and optoelectronic devices. The exchange of bulky and insulating organic surfactants with small inorganic ligands such as $In_2Se_4^{2-}$, $Cu_7S_4^{2-}$, $Sn_2S_6^{4-}$, and $Sn_2Se_6^{4-}$ facilitated the electronic coupling between individual III−V NCs. Similar behavior was recently observed for CdSe NCs capped with $In_2Se_4^{2-}$ and $Sn_2Se_6^{4-}$ ligands.[17,19,22] For charge transport studies, the films of InAs NCs and InP NCs were annealed at 200−250 °C on a hot-plate or at 350 °C for 5−15 s using RTA.

Figure 3a,b shows representative output and transfer characteristics for an FET device with channel assembled of 4.5 nm InAs NCs capped with $Cu_7S_4^-$ MCC ligands annealed at 350 °C for 5 s using RTA. The thickness of the NC layers was 25−30 nm, which exceeded the depth of the accumulation

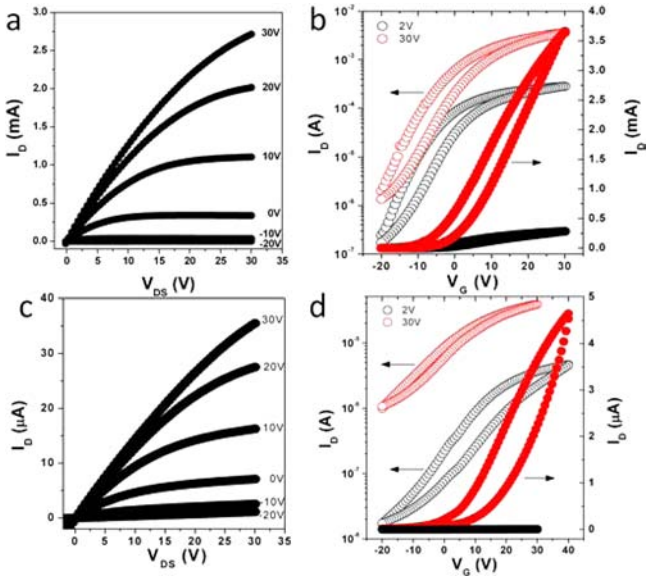

Figure 3. Output and transfer characteristics of FETs made of III−V NCs. (a) Plots of the drain current (I_D) vs drain-source voltage (V_{DS}) measured at different gate voltages (V_G). (b) Plots of I_D vs V_G used to calculate current modulation and electron mobility at constant V_{DS} = 2 V for the linear regime and V_{DS} = 30 V for the saturation regime for a n-type FET assembled from 4.5 nm InAs NCs capped with $Cu_7S_4^-$ ligands. (c) I_D vs V_{DS} plots measured for different V_G values, and (d) I_D vs V_G at V_{DS} = 2 V and V_{DS} = 30 V for FETs assembled from 4.0 nm InP NCs capped with $Sn_2S_6^{4-}$. The channel length and width are 150 μm and 1500 μm, respectively. The thickness of the SiO_2 gate oxide is 100 nm.

channel formed in the NC layer upon applied gate bias.[34,35] The drain current (I_D) versus drain-source voltage (V_{DS}) scans at different gate voltages (V_G) as well as I_D versus V_G scans show behaviors typical for a n-type semiconductor. What makes these devices remarkable is the electron mobility that approached 16 $cm^2/(V\ s)$ in the linear regime and 14.8 $cm^2/(V\ s)$ in the saturation regime of FET operation. Figures S8 and S9 (Supporting Information) show the typical output and transfer characteristics for FETs assembled from InAs NCs capped with different MCC ligands and annealed at 200 °C for 1 h using a hot-plate and at 350 °C for 5 s using RTA, respectively. Observed electron mobility and current modulations are summarized in Table 1. The mobility values observed for the arrays of MCC-capped InAs NCs are many orders of magnitude higher than those previously reported for III−V NC solids[5,12] and are among the highest reported for NC FETs.[22,23,36] For all of the MCC ligands, the mobility generally increased with increasing annealing temperature, with the best performance observed for devices annealed using RTA. It is known that trapping of electrons at the surface of SiO_2 gate dielectric can affect the subthreshold slope and cause hysteresis to the transfer characteristics of NC FETs.[30] This problem can be addressed by using more sophisticated gate dielectrics.[30,36] However, in this study, we focused on new channel materials and tried to avoid all possible sources of chemical interference. For this reason, we used the most straightforward device layout yet providing accurate estimations for field-effect carrier mobility.

The FET devices made of MCC-capped InP NCs also showed n-type gate effect (Figures 3c,d and S10 (Supporting Information)). The measured values of electron mobility for

Table 1. Summary of FET Parameters[a]

NC	ligand	heat treatment regime (°C/time)	mobility ($cm^2/(V\ s)$) lin	mobility ($cm^2/(V\ s)$) sat	on/off ratio	thickness of NC layer (nm)
InAs NCs	$Cu_7S_4^-$	350/RTA	16.0	14.8	$\sim10^3$	~27 nm
		200/30 min	3.48	N/A	$\sim10^3$	
	$Sn_2S_6^{4-}$	350/RTA	3.96	1.77	10^1-10^2	
		200/30 min	0.61	0.27	10^2-10^3	
	$Sn_2Se_6^{4-}$	350/RTA	1.9	0.9	10^1-10^2	
		200/30 min	0.33	0.39	10^2-10^3	
	$In_2Se_4^{2-}$	350/RTA	3.35	0.72	~10	
	S^{2-}	250/30 min	0.85	0.6	$\sim10^3$	
InP NCs	$Sn_2S_6^{4-}$	350/RTA	0.09	0.05	$\sim10^2$	~24 nm
	$Sn_2Se_6^{4-}$	350/RTA	0.07	0.04	10^2-10^3	
	$In_2Se_4^{2-}$	250/30 min	2×10^{-4}	1.2×10^{-3}	$\sim10^3$	

[a] μ_{lin} and μ_{sat} are the linear and saturation mobility, respectively.

InP-based FETs were significantly lower than those observed for InAs NCs (Table 1). We currently do not have a satisfactory explanation of this difference in electron mobility between InP and InAs NCs. Most likely, the surface of MCC-capped InP NCs can trap charge carriers thus reducing their ability to move under an applied electric field. At the same time, in FET devices, mobility depends both on the intrinsic property of the channel material (particle size, monodispersity, etc.) and on a number of device parameters (gate dielectric, contacts, etc.). These are all reasons to expect that a higher performance of III–V NC solids will be obtained after further optimization of the FET devices.

To provide an additional insight into the mechanism of charge transport in the arrays of InAs NCs bridged with inorganic ligands, we studied the effect of temperature on the electron mobility. In the case of weakly coupled NCs, charge transport typically occurs in the hopping regime, and conductivity (σ) drops at low temperatures following the hopping relation $\sigma \sim \exp(1/T^{\nu})$, where ν depends on the activation energy, dimensionality, and Coulombic interactions in the NC solid (ν equals 1 for near-neighbor hopping, $^1/_2$ for Efros–Shklovskii variable-range hopping, and $^1/_4$ for Mott variable-range hopping in a three-dimensional material).[23] Such temperature dependence has been observed in the films of InAs NCs capped with $Sn_2S_6^{4-}$ ligands that showed rather low electron mobility (Figure S11, Supporting Information).

The NC FET devices using InAs NCs capped with $Cu_7S_4^-$ ligands reproducibly showed electron mobility above 10 $cm^2/(V\ s)$. In parallel with such high mobility, we observed nearly temperature-independent mobility across the 80–300 K temperature range (Figure 4). Thus, in the linear regime of FET operation, at small source-drain voltage (3 V applied across a 150 μm long channel or ~0.1 mV per 5 nm diameter NC), the mobility decreased from 12.6 $cm^2/(V\ s)$ at 300 K to 11.4 $cm^2/(V\ s)$ at 80 K that corresponded to an effective activation energy E_a of ~1 meV. This number is very small and suggests that the system is on the edge of switching from activated transport to some different conduction mechanism. When we increased the source-drain voltage to 30 V (~1 mV across the NC), the temperature coefficient of mobility, $d\mu/dT$, changed sign from positive to negative as shown in Figure 4. Transport with $d\mu/dT < 0$ is typically called "bandlike transport",[36,37] which however, does not directly imply the formation of a three-dimensional band. For example, in some organic semiconductors, bandlike transport at large source-drain voltages occurs via with the downfield hopping through localized states.[37]

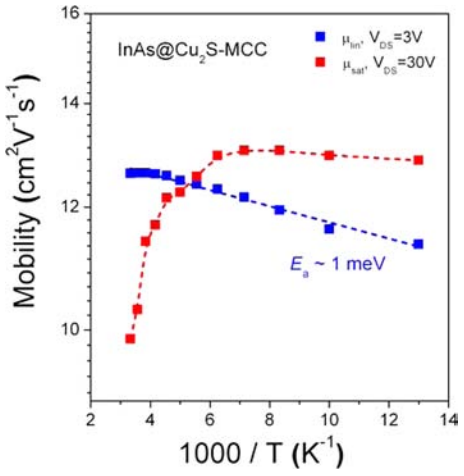

Figure 4. Temperature dependence for the field-effect electron mobility in the films of InAs NCs capped with $Cu_7S_4^-$ MCC ligands annealed at 350 °C for 5 s. Blue squares correspond to the linear regime of FET operation (μ_{lin} measured at 3 V source-drain voltage applied across a 150 μm long channel). Red squares correspond to the saturation regime of FET operation (μ_{sat} measured 30 V source-drain voltage applied across a 150 μm long channel).

In general, the electron transport in MCC-capped InAs NC solids agrees well with the behavior of disordered semiconductors and granular electronic systems.[38,39] In such systems, disorder and Coulomb charging energy force localization of charge carriers whereas exchange coupling energy between individual NCs promotes formation of extended electronic states where carriers are delocalized across multiple NCs. Depending on the interplay between the coupling energy determined primarily by ligands on one side and disorder coming from NC size distribution and packing morphology, the wave functions can localize on individual NCs (weak coupling limit) or form extended states—minibands—corresponding to the limit of the strongly coupled NC solid. According to Levine et al., the transition between these limiting cases should occur through the stage where NC wave functions couple over finite domains.[40] In that case, transport between the domains can still occur via hopping. Recent observation of high electron mobility (>10 $cm^2/(V\ s)$) with bandlike temperature dependence in films of MCC-capped CdSe NCs at low source-drain bias[22,36] strongly suggests the formation of some kind of extended

electronic states, since such high μ values cannot be easily explained via electron hopping between localized states.[36] The picture of domain localization can also explain nonmonotonic temperature dependence of mobility with $d\mu/dT < 0$ at high temperatures and $d\mu/dT > 0$ at low temperatures (see, e.g., the red curve in Figure 4 and ref 36). At high temperatures, the interdomain hopping is fast, and transport within the domains can dominate film conductivity. The rate of charge hopping between domains drops exponentially with temperature and creates a transport bottleneck with $d\mu/dT > 0$ below a certain temperature.

3.3. Photoconductivity in the Arrays of MCC-capped InAs and InP NCs. To illuminate the NC samples, we used laser diodes controlled by a laser driver (Thorlabs, DC205C) and signal generator (SRS, DS-345). The photoresponse of close-packed films of InP or InAs NCs capped with various MCC ligands was measured at four different wavelengths: 650 nm (1.91 eV, 0.51 mW/cm^2), 980 nm (1.27 eV, 0.26 mW/cm^2), 1310 nm (0.95 eV, 0.48 mW/cm^2), and 1550 nm (0.80 eV, 0.47 mW/cm^2). We also varied carrier concentration in the NC films by applying gate voltage (Figure 5a) either under nitrogen atmosphere or in vacuum at different temperatures between 100 and 300 K.

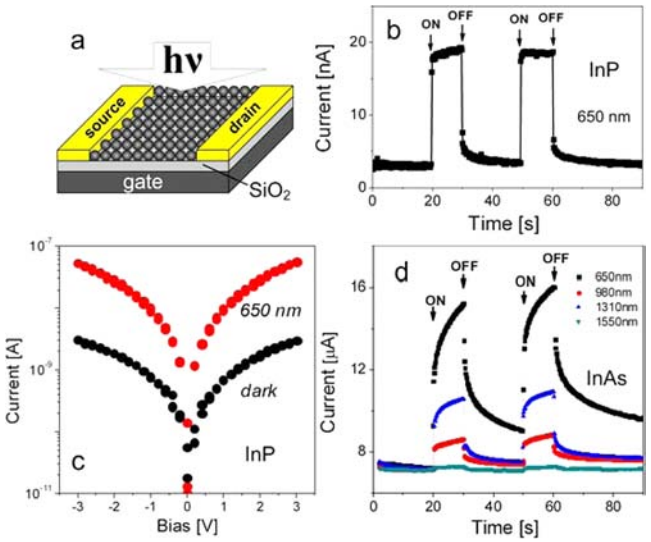

Figure 5. Photoresponse of the films of InP and InAs NCs capped with $In_2Se_4^{2-}$ ligands. (a) Schematics of the experimental setup for photoconductivity measurements. (b) Illumination with 650 nm light results in the increase of conductivity of the film of $Sn_2Se_6^{4-}$-capped 4.0 nm InP NCs. The photoresponse was measured at a bias of 2 V applied across a 4.5 μm channel. (c) Bias dependence for dark current and photocurrent across the film of $Sn_2Se_6^{4-}$-capped 4.0 nm InP NCs. (d) Photoresponse measured at different excitation wavelengths for a film of 4.5 nm InAs NCs capped with $In_2Se_4^{2-}$ ligands at a bias of 2 V applied across as a 150 μm long channel.

Figure 5b,c shows the photoresponse of a film of $In_2Se_4^{2-}$-capped 4.0 nm InP NCs annealed at 250 °C for 30 min. The increase of the current flowing through the NC film under constant bias was observed upon illumination at 650 nm that closely matched the position of the first excitonic peak of InP NCs. The magnitude of the photocurrent was proportional to the bias applied to the InP NC film. No photocurrent was observed when the photon energy was lower than the NC band gap, since photon energy was not sufficient to generate electron–hole pairs. Qualitatively similar behavior was observed for InP NCs capped with $Sn_2S_6^{4-}$ and $Sn_2Se_6^{4-}$ ligands (Figure S12, Supporting Information). Such an increase of conductivity under illumination is very typical for arrays of semiconductor NCs and has been observed for II–VI (e.g., CdSe,[12,41–43] CdTe,[44] HgTe,[45] CdSe/CdS,[22] and CdSe/ZnS[13] core–shells, etc.) and IV–VI (PbS[46] and PbSe[47]) NCs.

The arrays of MCC-capped InAs NCs showed distinctively different behavior under illumination. The first set of measurements was carried out for InAs NCs capped with $In_2Se_4^{2-}$, $Cu_7S_4^-$, $Sn_2S_6^{4-}$, and $Sn_2Se_6^{4-}$ ligands and annealed at 200 °C for 1 h. Figure 5d shows the photocurrent response to chopped illumination with different photon energies for the film of $In_2Se_4^{2-}$-capped InAs NCs measured at constant 2 V bias applied across a 4.5 μm channel. We observed a positive photoresponse for all four wavelengths. The absorption of the NC layer increased with increasing the photon energy since more carriers were promoted from the $1S_h$ highest occupied state to the $1S_e$ lowest unoccupied state in a thin NC layer upon excitation at shorter wavelength. As a result, the magnitude of the photocurrent at comparable photon flux increased upon decreasing the excitation wavelength, as shown in Figure S13 (Supporting Information) where photocurrent was normalized for the photon flux as different wavelengths. Such behavior was commonly observed in different NC solids.[41,47,48]

Qualitatively different behavior has been observed for the photoconductivity of InAs NCs capped with $Cu_7S_4^-$, $Sn_2S_6^{4-}$, and $Sn_2Se_6^{4-}$ ligands. Figure 6a,b shows the photocurrent response of 4.5 nm InAs NCs capped with $Cu_7S_4^-$ and $Sn_2S_6^{4-}$ ligands, respectively, to chopped illumination with different wavelengths. These NCs showed excitonic absorption transitions in the near-IR range (Figures 1b and 2c). When illuminated close to the absorption onset, for example, at 0.80 and 0.95 eV, these NC solids showed expected positive photocurrent response. However, when the photon energy increased to 1.27 and 1.91 eV, we observed a transition from positive to a *negative* photoresponse! We also studied the effect of gate voltage on photoconductivity of thin films of MCC-capped InAs NCs. When excited close to the absorption onset (0.95 eV), a positive photocurrent was observed for all V_G values between −20 V and 20 V (Figure S14, Supporting Information). At the same time, under excitation at 1.27 eV (980 nm), we observed a negative photoresponse at $V_G < 3$ V and a positive photoresponse at $V_G > 3$ V as shown in Figure 6c. The photoresponse also changed sign from negative to positive when the light intensity exceeded some threshold. The threshold intensity decreased with decreasing temperature. For example, for a film of 4.5 nm InAs NCs capped with $Sn_2S_6^{4-}$ ligands, we observed a switching from negative to positive photoresponse at ~0.05 mW/cm^2 at 100 K in vacuum (Figures 6d and S15 (Supporting Information)). Depending on the particular MCC, a rich variety of transient responses upon off-to-on and on-to-off illumination switching was observed. In the further analysis, we primarily focus on the steady-state (persistent) photoresponse related to the carrier generation/recombination dynamics. Transient photoconductivity probably reflects the capacitive response of the states at the NC surface or MCC ligands, which should be a subject of a separate study.

Negative photoconductivity is uncommon and to the best of our knowledge has not been reported for semiconductor NCs. Occasionally, it has been observed in bulk semiconductors with deep trap states (e.g., Co-doped Si and Au-doped Ge).[17–23]

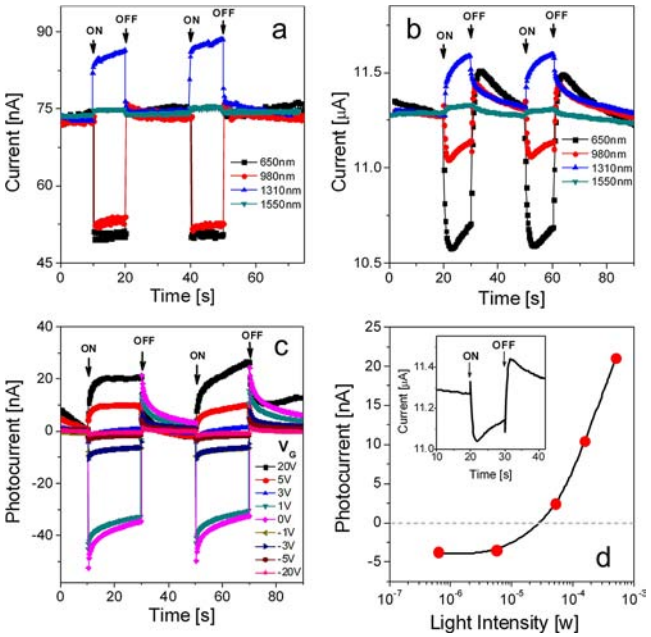

Figure 6. Ambipolar photoresponse of inorganically capped InAs NC arrays. (a, b) Photoresponse measured at 2 V bias at different excitation wavelengths for the films of 4.5 nm InAs NCs capped with (a) $Cu_7S_4^-$ and (b) $Sn_2S_6^{4-}$ ligands. (c) Photoresponse measured at a constant 2 V bias at different applied back-gate voltages for a film of $Sn_2S_6^{4-}$-capped 4.5 nm InAs NCs under excitation with 980 nm light. (d) Dependence of the photocurrent on the illumination intensity at 650 nm for a film of $Sn_2S_6^{4-}$-capped 4.5 nm InAs NCs. The inset shows a transient photoresponse for the same film upon switching 980 nm illumination on and off. All NC films were annealed at 200 °C for 1 h. The channel length and width are 150 μm and 1500 μm, respectively. The thickness of the SiO_2 gate oxide is 100 nm.

Stöckman[49] in 1955 and Johnson and Levinstein[50] in 1960 explained negative photoconductivity in Au-doped Ge using a model with two types of deep midgap states (lower and upper impurity levels). The dynamics of carrier trapping and recombination at these levels resulted in the negative photoresponse upon extrinsic excitation (i.e., below the fundamental absorption edge, $h\nu < E_g$) while intrinsic excitation with $h\nu > E_g$ resulted in normal (positive) photoconductivity.[50] A similar effect, with the surface states playing a role of deep impurity levels, has been observed in Bi-doped ZnSe nanowires.[51] This behavior is opposite to the one observed in arrays of MCC-capped InAs NCs, where negative photoresponse was observed at short wavelengths. Negative photoresponse has been recently reported for the films of Au NCs capped with charged thiolate ligands.[52] It was explained by photoinduced trapping of mobile electrons on polaron-like states within charged organic ligands. That model would be suitable for metal NCs with a high concentration of carriers at the Fermi level, but it cannot explain negative photoconductivity observed exclusively in InAs NCs and absent in other NCs capped with the same MCC ligands.

InAs/AlSb quantum well (QW) heterostructures have demonstrated the photoresponse similar to that shown in Figure 6a,b. For example, this QW system showed persistent positive photoconductance when illuminated below ~1.55 eV and negative photoconductance when illuminated above ~1.55 eV.[53] The switching occurred when the photon energy was sufficient for direct excitation of the AlSb layer. The holes generated in AlSb recombined with highly mobile electrons in InAs QWs thus reducing the conductivity. Compared to traditional organic ligands with very large HOMO−LUMO gaps, the MCCs form semiconducting barriers between individual NCs.[19] The arrays of MCC-capped InAs NCs could therefore behave similar to the QW superlattices in a way that the carrier could be photogenerated both in InAs QDs and in the inter-NC barriers. We cannot rule out this mechanism, but we have one line of evidence that MMC ligands do not play a key role in the negative photoconductivity of InAs NC films. We found that InAs NCs treated with pure DMF without any MCC ligands also showed switching from positive to negative photoresponse between 0.95 and 1.27 eV (Figure S16, Supporting Information).

The surface of bulk InAs has a unique feature: it has unusually high density of donorlike surface states that pin the Fermi level ~0.15 eV above the conduction band minimum.[54,55] These states were also observed at the InAs surface treated with S^{2-} ions,[56] similar to the bonding in MCC-capped InAs NCs. In a bulk semiconductor, it results in the formation of a degenerate accumulation layer with approximate width $W_{acc} = \sqrt{2L_D\{\exp(eV_{bi}/2k_BT) - 1\}}$, where V_{bi} is the built-in voltage and $L_D = (\varepsilon\varepsilon_0 k_B T/e^2 N_D)^{1/2}$ is the Debye screening length (ε is static dielectric constant, ε_0 is the vacuum permittivity, k_B is the Boltzmann constant, T is the temperature, e is the elemental charge, and N_D is the concentration of ionized donors in semiconductor).[57] For all reasonable ranges of V_{bi} and N_D, W_{acc} greatly exceeds the radius of InAs NCs used in this work, thus ruling out the possibility of band bending inside individual NCs. Instead, the donorlike state at the InAs−MCC interface should form a localized level (D_{ss}), presumably above the $1S_e$ state of InAs NCs as shown in Figure 7. The

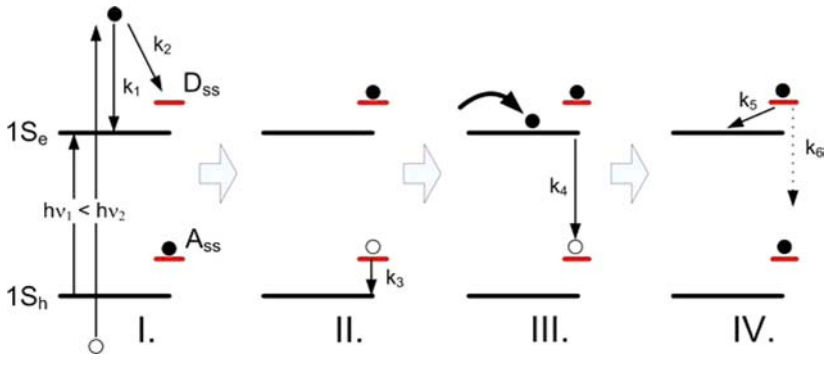

Figure 7. Scheme proposed to explain the ambipolar photoresponse of MCC-capped InAs NC solids. See the text for details.

dx.doi.org/10.1021/ja308200f | J. Am. Chem. Soc. 2013, 135, 1349−1357

optical absorption and dark transport measurements suggest that this state does not pin the Fermi level of InAs NCs above the $1S_e$ state; otherwise, suppressed excitonic features in the absorption spectra[58] and high dark conductivity of InAs NC films were observed. Most probably, the D_{ss} state is at least partially empty while released electrons are captured by the acceptor states at the NC surface or in the MCC barrier. When excited close to the absorption onset, the D_{ss} state cannot be additionally populated by charge carriers and remain silent. As a result, normal (positive) photoresponse is observed upon illumination at 0.80 and 0.95 eV.

To explain experimentally observed persistent negative photoconductivity in MCC-capped InAs NC solids under 1.27 and 1.91 eV illumination, we propose a modified Stöckman model,[49] where the upper impurity level (D_{ss}) is located *above the mobility edge* as shown in Figure 7. This model can result in a characteristic transient behavior shown in the inset to Figure 6d. When the illumination is turned on, it generates hot electrons that could either undergo intraband cooling (k_1 in Figure 7)[59] or get trapped at the D_{ss} level (k_2). Such competition between cooling and trapping for hot electrons has been recently observed in single-NC blinking experiments.[60] At the same time, photogenerated holes give a short burst of positive photoconductivity before trapping by the acceptor-type surface states A_{ss} originally filled with electrons (k_3 in Figure 7). Next, a mobile electron (e.g., from an ionized shallow donor) is recombined with the hole on A_{ss} (k_4) thus decreasing conductivity below the dark level (step III in Figure 7). The electron trapped by the D_{ss} state can either relax into the conduction band (k_5) or nonradiatively recombine with an empty acceptor state with the rate constant k_6. When the light is turned off, holes are no longer created thus further decreasing the conductivity for a short period of time until electrons get released from the D_{ss} state and the conductivity is restored to the dark level. We observed such photocurrent transients in some samples of 4.5 nm InAs NCs capped with $Sn_2S_6^{4-}$ ligands (inset to Figure 6d). In other samples, however, the capacitive response of the surface states filtered out fast components of transient photoresponse of the NC films.

Our model can explain why positive gate voltage can change the sign of the photocurrent from negative to positive (Figure 6c). When $V_G > 0$, additional electrons are pulled into the conduction channel thus raising the Fermi level above the mobility edge that should be close to the $1S_e$ state of InAs NCs.[36] The raising of the Fermi level above the mobility edge should also increase the population of the D_{ss} level and thus reduce the probability of trapping a hot electron by this state. The occupation of the D_{ss} level also increases at high illumination intensities, also causing switching from negative to positive photoresponse (Figure 6d). In the case of InAs NCs capped with $In_2Se_4^{2-}$ MCCs, we observed positive photoresponse at all wavelengths that can be explained by strong n-type doping, similar to that achieved at $V_G \gg 0$ for the NCs capped with other MCC ligands. Such high doping density is also evident from high dark conductivity and poor on/off ratio for FETs made of the $In_2Se_4^{2-}$-capped InAs NCs (Table 1 and Figures 5d and S9 (Supporting Information)).

4. SUMMARY

We demonstrated that various molecular chalcogenide ligands can strongly bind to the surface of InP and InAs NCs and stabilize their colloidal solutions in various polar solvents. The arrays of MCC-capped InAs NCs showed high field-effect electron mobility exceeding 10 $cm^2/(V\ s)$ that placed them on the list of prospective solution processed semiconductors for electronic and optoelectronic applications. The cadmium-free and lead-free nature of III–V semiconductors provides an additional benefit for their practical applications. In addition to high electron mobility, InAs NCs capped with MCC ligands showed rich ambipolar photoresponse where photoconductivity could be switched from positive to negative by changing the illumination wavelength or the carrier density on the NC solid.

■ ASSOCIATED CONTENT

Supporting Information

Additional experimental details, figures, and tables as described in the text. This material is available free of charge via the Internet at http://pubs.acs.org.

■ AUTHOR INFORMATION

Corresponding Author

dvtalapin@uchicago.edu

Author Contributions

[§]These authors contributed equally to this work.

Notes

The authors declare no competing financial interest.

■ ACKNOWLEDGMENTS

The work on synthesis and characterization of MCC-capped NCs was supported by NSF CAREER under award no. DMR-0847535; the work on charge transport and photoconductivity in NC solids was supported by the DOE SunShot program under award no. DE-EE0005312. D.V.T. also thanks the David and Lucile Packard Foundation and the Keck Foundation for their generous support. This work used facilities supported by the NSF MRSEC program under award no. DMR-0213745. Inductively coupled plasma/optical emission spectroscopy elemental analysis was carried out at the Analytical Chemistry Laboratory at Argonne National Lab (ANL). The work at the Center for Nanoscale Materials (ANL) was supported by the U.S. Department of Energy under contract no. DE-AC02-06CH11357.

■ REFERENCES

(1) Hoff, J.; He, X.; Erdtmann, M.; Bigan, E.; Razeghi, M.; Brown, G. J. *J. Appl. Phys.* **1995**, *78*, 2126–2128.

(2) Bandyopadhyay, N.; Slivken, S.; Bai, Y.; Razeghi, M. *Appl. Phys. Lett.* **2012**, *100*, 212104–4.

(3) Hoang, A. M.; Chen, G.; Haddadi, A.; Pour, S. A.; Razeghi, M. *Appl. Phys. Lett.* **2012**, *100*, 211101–4.

(4) Geyer, S. M.; Allen, P. M.; Chang, L.-Y.; Wong, C. R.; Osedach, T. P.; Zhao, N.; Bulovic, V.; Bawendi, M. G. *ACS Nano* **2011**, *4*, 7373–7378.

(5) Soreni-Harari, M.; Mocatta, D.; Zimin, M.; Gannot, Y.; Banin, U.; Tessler, N. *Adv. Funct. Mater.* **2010**, *20*, 1005–1010.

(6) Ziegler, J.; Xu, S.; Kucur, E.; Meister, F.; Batentschuk, M.; Gindele, F.; Nann, T. *Adv. Mater.* **2008**, *20*, 4068–4073.

(7) Tessler, N.; Medvedev, V.; Kazes, M.; Kan, S.; Banin, U. *Science* **2002**, *295*, 1506–1508.

(8) Murray, C. B.; Kagan, C. R.; Bawendi, M. G. *Annu. Rev. Mater. Sci.* **2000**, *30*, 545.

(9) Kuno, M.; Lee, J. K.; Dabbousi, B. O.; Mikulec, F. V.; Bawendi, M. G. *J. Chem. Phys.* **1997**, *106*, 9869–9882.

(10) Talapin, D. V.; Murray, C. B. *Science* **2005**, *310*, 86–89.

(11) Gur, I.; Fromer, N. A.; Geier, M. L.; Alivisatos, A. P. *Science* **2005**, *310*, 462–465.

(12) Oertel, D. C.; Bawendi, M. G.; Arango, A. C.; Bulovic, V. *Appl. Phys. Lett.* **2005**, *87*, 213505−3.
(13) Porter, V. J.; Geyer, S.; Halpert, J. E.; Kastner, M. A.; Bawendi, M. G. *J. Phys. Chem. C* **2008**, *112*, 2308−2316.
(14) Webber, D. H.; Brutchey, R. L. *J. Am. Chem. Soc.* **2012**, *134*, 1085−1092.
(15) Luther, J. M.; Law, M.; Song, Q.; Perkins, C. L.; Beard, M. C.; Nozik, A. J. *ACS Nano* **2008**, *2*, 271−280.
(16) Zarghami, M. H.; Liu, Y.; Gibbs, M.; Gebremichael, E.; Webster, C.; Law, M. *ACS Nano* **2010**, *4*, 2475−2485.
(17) Guzelian, A. A.; Banin, U.; Kadavanich, A. V.; Peng, X.; Alivisatos, A. P. *Appl. Phys. Lett.* **1996**, *69*, 1432−1434.
(18) Geyer, S. M.; Allen, P. M.; Chang, L.-Y.; Wong, C. R.; Osedach, T. P.; Zhao, N.; Bulovic, V.; Bawendi, M. G. *ACS Nano* **2010**, *4*, 7373−7378.
(19) Kovalenko, M. V.; Scheele, M.; Talapin, D. V. *Science* **2009**, *324*, 1417−1420.
(20) Kovalenko, M. V.; Bodnarchuk, M. I.; Zaumseil, J.; Lee, J. S.; Talapin, D. V. *J. Am. Chem. Soc.* **2010**, *132*, 10085−10092.
(21) Fafarman, A. T.; Koh, W. K.; Diroll, B. T.; Kim, D. K.; Ko, D. K.; Oh, S. J.; Ye, X. C.; Doan-Nguyen, V.; Crump, M. R.; Reifsnyder, D. C.; Murray, C. B.; Kagan, C. R. *J. Am. Chem. Soc.* **2011**, *133*, 15753−15761.
(22) Lee, J. S.; Kovalenko, M. V.; Huang, J.; Chung, D. S.; Talapin, D. V. *Nat. Nanotechnol.* **2011**, *6*, 348−352.
(23) Talapin, D. V.; Lee, J. S.; Kovalenko, M. V.; Shevchenko, E. V. *Chem. Rev.* **2010**, *110*, 389−458.
(24) Battaglia, D.; Peng, X. *Nano Lett.* **2002**, *2*, 1027−1030.
(25) Baek, J.; Allen, P. M.; Bawendi, M. G.; Jensen, K. F. *Angew. Chem., Int. Ed.* **2011**, *50*, 627−630.
(26) Mitzi, D. B.; Copel, M.; Chey, S. J. *Adv. Mater.* **2005**, *17*, 1285−1289.
(27) Mitzi, D. B.; Kosbar, L. L.; Murray, C. E.; Copel, M.; Afzali, A. *Nature* **2004**, *428*, 299−303.
(28) Mitzi, D. B. *Inorg. Chem.* **2007**, *46*, 926−931.
(29) Milliron, D. J.; Mitzi, D. B.; Copel, M.; Murray, C. E. *Chem. Mater.* **2006**, *18*, 587−590.
(30) Chung, D. S.; Lee, J.-S.; Huang, J.; Nag, A.; Ithurria, S.; Talapin, D. V. *Nano Lett.* **2012**, *12*, 1813−1820.
(31) Dong, A.; Ye, X.; Chen, J.; Kang, Y.; Gordon, T.; Kikkawa, J. M.; Murray, C. B. *J. Am. Chem. Soc.* **2011**, *133*, 998−1006.
(32) Nag, A.; Kovalenko, M. V.; Lee, J.-S.; Liu, W.; Spokoyny, B.; Talapin, D. V. *J. Am. Chem. Soc.* **2011**, *133*, 10612−10620.
(33) Adam, S.; Talapin, D. V.; Borchert, H.; Lobo, A.; McGinley, C.; de Castro, A. R. B.; Haase, M.; Weller, H.; Moller, T. *J. Chem. Phys.* **2005**, *123*, 084706−10.
(34) Tessler, N.; Preezant, Y.; Rappaport, N.; Roichman, Y. *Adv. Mater.* **2009**, *21*, 2741−2761.
(35) Mentzel, T. S.; Porter, V. J.; Geyer, S.; MacLean, K.; Bawendi, M. G.; Kastner, M. A. *Phys. Rev. B* **2008**, *77*, 075316.
(36) Choi, J.-H.; Fafarman, A. T.; Oh, S. J.; Ko, D.-K.; Kim, D. K.; Diroll, B. T.; Muramoto, S.; Gillen, J. G.; Murray, C. B.; Kagan, C. R. *Nano Lett.* **2012**, *12*, 2631−2638.
(37) Sakanoue, T.; Sirringhaus, H. *Nat. Mater.* **2010**, *9*, 736−740.
(38) Beloborodov, I. S.; Lopatin, A. V.; Vinokur, V. M.; Efetov, K. B. *Rev. Mod. Phys.* **2007**, *79*, 469−518.
(39) Shklovskii, B. I.; Efros, A. L. *Electronic Properties of Doped Semiconductors*; Springer-Verlag: Berlin, Germany, 1984.
(40) Beverly, K. C.; Sample, J. L.; Sampaio, J. F.; Remacle, F.; Heath, J. R.; Levine, R. D. *Proc. Natl. Acad. Sci. U.S.A.* **2002**, *99*, 6456−6459.
(41) Leatherdale, C. A.; Kagan, C. R.; Morgan, N. Y.; Empedocles, S. A.; Kastner, M. A.; Bawendi, M. G. *Phys. Rev. B* **2000**, *62*, 2669−2680.
(42) Jarosz, M. V.; Porter, V. J.; Fisher, B. R.; Kastner, M. A.; Bawendi, M. G. *Phys. Rev. B* **2004**, *70*, 195327.
(43) Yu, D.; Wehrenberg, B. L.; Jha, P.; Ma, J.; Guyot-Sionnest, P. *J. Appl. Phys.* **2006**, *99*, 104315−7.
(44) Porter, V. J.; Mentzel, T.; Charpentier, S.; Kastner, M. A.; Bawendi, M. G. *Phys. Rev. B* **2006**, *73*, 155303.
(45) Keuleyan, S.; Lhuillier, E.; Brajuskovic, V.; Guyot-Sionnest, P. *Nat. Photonics* **2011**, *5*, 489−493.
(46) Konstantatos, G.; Sargent, E. H. *Appl. Phys. Lett.* **2007**, *91*, 173505−3.
(47) Konstantatos, G.; Howard, I.; Fischer, A.; Hoogland, S.; Clifford, J.; Klem, E.; Levina, L.; Sargent, E. H. *Nature* **2006**, *442*, 180−183.
(48) Konstantatos, G.; Sargent, E. H. *Nat. Nanotechol.* **2010**, *5*, 391−400.
(49) Stöckmann, F. *Z. Phys.* **1955**, *143*, 348−356.
(50) Johnson, L.; Levinstein, H. *Phys. Rev.* **1960**, *117*, 1191−1203.
(51) Zhang, X.; Jie, J.; Wang, Z.; Wu, C.; Wang, L.; Peng, Q.; Yu, Y.; Jiang, P.; Xie, C. *J. Mater. Chem.* **2011**, *21*, 6736−6741.
(52) Nakanishi, H.; Bishop, K. J. M.; Kowalczyk, B.; Nitzan, A.; Weiss, E. A.; Tretiakov, K. V.; Apodaca, M. M.; Klajn, R.; Stoddart, J. F.; Grzybowski, B. A. *Nature* **2009**, *460*, 371−375.
(53) Gauer, C.; Scriba, J.; Wixforth, A.; Kotthaus, J. P.; Nguyen, C.; Tuttle, G.; English, J. H.; Kroemer, H. *Semicond. Sci. Technol.* **1993**, *8*, S137.
(54) Olsson, L. O.; Andersson, C. B. M.; Hakansson, M. C.; Kanski, J.; Ilver, L.; Karlsson, U. O. *Phys. Rev. Lett.* **1996**, *76*, 3626−3629.
(55) Weber, J. R.; Janotti, A.; Walle, C. G. V. d. *Appl. Phys. Lett.* **2010**, *97*, 192106.
(56) Petrovykh, D. Y.; Yang, M. J.; Whitman, L. J. *Surf. Sci.* **2003**, *523*, 231−240.
(57) Sze, S. M. *Semiconductor Devices: Physics and Technology*; John Wiley and Sons: New York, 2002.
(58) Shim, M.; Guyot-Sionnest, P. *Nature* **2000**, *407*, 981−983.
(59) Guyot-Sionnest, P.; Wehrenberg, B.; Yu, D. *J. Chem. Phys.* **2005**, *123*, 074709.
(60) Galland, C.; Ghosh, Y.; Steinbruck, A.; Sykora, M.; Hollingsworth, J. A.; Klimov, V. I.; Htoon, H. *Nature* **2011**, *479*, 203−207.